INTERNATIONAL JOURNAL FOR NUMERICAL METHODS IN FLUIDS
Int. J. Numer. Meth. Fluids **29**: 375–387 (1999)

2D SHALLOW WATER FLOW MODEL FOR THE HYDRAULIC JUMP

J.G. ZHOU* AND P.K. STANSBY

Hydrodynamics Research Group, School of Engineering, The University, Manchester M13 9PL, UK

SUMMARY

A flow model is presented for predicting a hydraulic jump in a straight open channel. The model is based on the general 2D shallow water equations in strong conservation form, without artificial viscosity, which is usually incorporated into the flow equations to capture a hydraulic jump. The equations are discretised using the finite volume method. The results are compared with experimental data and available numerical results, and have shown that the present model can provide good results. The model is simple and easy to implement. To demonstrate the potential application of the model, several hydraulic jumps occurring in different situations are simulated, and the predictions are in good agreement with standard solution for open channel hydraulics. Copyright © 1999 John Wiley & Sons, Ltd.

KEY WORDS: shallow water flow; finite volume method; hydraulic jump; open channel flow

1. INTRODUCTION

The hydraulic jump is a basic physical phenomenon in natural river or open channel flows. It occurs when flow changes from a supercritical to a subcritical state. During this transition, there is strong turbulent mixing and energy dissipation. Such characteristics are often used for energy dissipation in hydraulic engineering [1].

Since Bélanger [2] studied the classical hydraulic jump and derived the Bélanger formula describing the conjugate depths in 1828, considerable experimental and theoretical research on hydraulic jumps has been carried out and reviewed by Hager [1], Chow [3] and Rajaratnam [4]. In recent years, with the development of computer hardware, numerical models for hydraulic jump prediction have attracted many researchers. This work may be classified into three categories: 1D model, 2D vertical model and 2D depth-averaged or shallow water model. In 1D models, the shallow water equations, sometimes with the Boussinesq term, are used to capture a hydraulic jump with either the finite difference method or the finite element method. Usually, an artificial viscosity is incorporated to suppress the oscillations due to steep gradients within the jump [5–7]. In 1995, Rahman and Chaudhry [8] numerically studied the hydraulic jump with grid adaptation. An artificial viscosity was still incorporated in the model to avoid the oscillations. One (or more) artificial viscosity coefficients will inevitably introduce uncertainty in a model.

* Correspondence to: Hydrodynamics Research Group, School of Engineering, Manchester University, Oxford Road, Manchester M13 9PL, UK.

CCC 0271–2091/99/040375–13$17.50

Received January 1996
Revised January 1998

In 2D vertical models, the Reynolds averaged Navier–Stokes equations are the basis of the models. This enables the models to predict the details of the flow pattern within the hydraulic jump. Long *et al.* [9] numerically investigated the submerged hydraulic jump using the offset control volume method, together with the standard k–ϵ closure for the eddy viscosity. The method was limited to flows over a plane bed with small surface slope. Chippada *et al.* [10] developed a model for a hydraulic jump in plane channels using the finite element method. They also considered the non-hydrostatic pressure within the jump by solving an additional Poisson's equation. There is no detailed comparison with experiments reported in the paper. The non-conservative equations used in the model may be another drawback [11]. Liu and Drewes [12] investigated the turbulence characteristics in free and forced hydraulic jumps, with the k–ϵ turbulence model. They compared the numerical results with experimental data from 1D laser-Doppler anemometry (LDA) for the downstream sections of the jump surface roller (Figure 1).

In a 2D depth-averaged or shallow water model, Younus and Chaudhry [13] simulated the hydraulic jump by using a depth-averaged k–ϵ model. An artificial viscosity is incorporated in the model to suppress the oscillations in the jump. Molls and Chaudhry [14] developed a depth-averaged model that can be used to predict a hydraulic jump. Also, the model includes an artificial viscosity. As indicated earlier, the artificial viscosity included in the model will introduce additional uncertainty and play the role of a fitting factor. In addition, the conservation feature of the flow equations is not guaranteed in these models. Recently, Khan and Steffler [15] proposed a physically based hydraulic jump model by carrying out a detailed analysis of the integral momentum conservation within hydraulic jump. They considered the characteristics at the middle of the jump based on the experiments of Rouse *et al.* [16] and introduced a jump flux, J, in the equations. The model gives improved results when compared with the shallow water equations for the jump.

To sum up, most existing models are either complex or especially developed for a hydraulic jump with an artificial viscosity. From the physical point of view, hydraulic jumps should be described by the same flow equations in all regions. Ideally, a same flow model can be used to simulate open channel flows, including complex phenomena such as hydraulic jump and hydraulic drop.

In this paper, the 2D shallow water flow model of Zhou [17] is applied to hydraulic jumps in straight rectangular open channels. The ability of the model to predict open channel flows has been demonstrated [17–19]. The main purpose here is to further test the validity of the same model in situations with hydraulic jumps. This will simplify the application of the model to practical engineering problems. The feature of the model is that it retains the same global conservation properties as the original flow equations. The solution method needs standard boundary conditions. The model is verified by comparison with experimental data and the other numerical results.

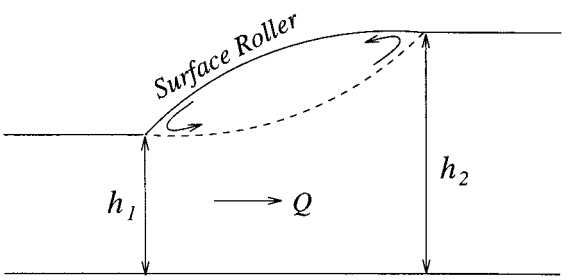

Figure 1. Sketch and notation for hydraulic jump.

2. GOVERNING EQUATIONS AND SOLUTIONS

2.1. Governing equations

The general governing equations for a steady 2D shallow water flow in Cartesian co-ordinates may be written in strong conservation form as [17]:

$$\frac{\partial(uh)}{\partial x}+\frac{\partial(vh)}{\partial y}=0, \tag{1}$$

$$\frac{\partial(uuh)}{\partial x}+\frac{\partial(vuh)}{\partial y}=-g\frac{\partial}{\partial x}\left(\frac{h^2}{2}\right)-gh\frac{\partial z_b}{\partial x}-\frac{\tau_{bx}}{\rho}+\frac{\partial}{\partial x}\left(hv_t\frac{\partial u}{\partial y}\right)+\frac{\partial}{\partial y}\left(hv_t\frac{\partial u}{\partial y}\right), \tag{2}$$

$$\frac{\partial(uvh)}{\partial x}+\frac{\partial(vvh)}{\partial y}=-g\frac{\partial}{\partial y}\left(\frac{h^2}{2}\right)-gh\frac{\partial z_b}{\partial y}-\frac{\tau_{by}}{\rho}+\frac{\partial}{\partial x}\left(hv_t\frac{\partial v}{\partial x}\right)+\frac{\partial}{\partial y}\left(hv_t\frac{\partial v}{\partial y}\right). \tag{3}$$

where x and y represent the Cartesian co-ordinates in the horizontal plane; u and v are the depth-averaged velocity components in the x- and y-directions; h is the water depth; z_b is the bed elevation above horizontal datum; ρ is the fluid density; v_t is the depth-averaged turbulence viscosity; τ_{bx} and τ_{by} are the bed shear stresses in the x- and y-directions.

It must be noted that the dispersion due to vertical non-uniformities of velocities in Equations (2) and (3) has been neglected. In most shallow water flows, velocity distribution over the depth is nearly uniform because of the strong turbulence effect. The errors caused by omission of the dispersion may be ignored in the results with little loss of accuracy [18,19].

τ_{bx} and τ_{by} are normally described by the depth-averaged velocities as

$$\tau_{bx}=\rho C_b u\sqrt{u^2+v^2}, \qquad \tau_{by}=\rho C_b v\sqrt{u^2+v^2}, \tag{4}$$

where C_b is the bed friction coefficient, which can be either constant or variable, calculated through the Chezy coefficient C_z as

$$C_b=\frac{g}{C_z^2}. \tag{5}$$

And C_z can be evaluated based on either the Manning equation:

$$C_z=\frac{h^{1/6}}{n}, \tag{6}$$

or the Colebrook–White equation [20]:

$$C_z=-\sqrt{32g}\log_{10}\left[\frac{K_s}{14.8h}+\frac{1.255vC_z}{4\sqrt{2g\,uh}}\right], \tag{7}$$

where n is the Manning coefficient and K_s is the Nikuradse equivalent sand roughness.

The depth-averaged turbulence viscosity v_t is given by Equation (8) based on a logarithmic velocity profile, assuming that bed-generated turbulence dominates over free shear layer turbulence [21].

$$v_t=\frac{k}{6}u_*h, \tag{8}$$

where k is the von Kármán constant ($=0.4$); and u_* is the shear velocity, which can be derived from Equation (4) as

$$u_*=\sqrt{C_b(u^2+v^2)}. \tag{9}$$

2.2. Features of the equations

The most important feature of Equations (1)–(3) is that they are strongly conservative. If the transverse velocity v, bottom shear stress τ_b and diffusion terms are neglected, integrating Equations (1) and (2) along the x-direction, from upstream to downstream of a hydraulic jump, leads to

$$u_1 h_1 = u_2 h_2 = q \tag{10}$$

and

$$u_2^2 h_2 - u_1^2 h_1 = -\frac{g}{2}(h_2^2 - h_1^2), \tag{11}$$

where subscripts 1 and 2 denote upstream and downstream of the jump respectively, as shown in Figure 1, and $q = hu$ is the discharge per unit width.

After defining the Froude number $Fr = u/\sqrt{gh}$, combining (10) and (11) results in

$$\frac{h_2}{h_1} = \frac{\sqrt{8Fr_1^2 + 1} - 1}{2}, \tag{12}$$

which is the Bélanger formula [4] and h_1 and h_2 are usually called conjugate or sequent depths.

Therefore, the flow model based on these equations can automatically be shock-capturing if the conservative feature is retained in the solution method. Since the finite volume approach is characterised by integrating Equations (1)–(3) over a finite number of control volumes, the resulting fluxes will cancel in pairs at all interior control volume faces. Hence, only boundary fluxes retain. This guarantees the same conservation of the transported quantity in the discretised equations as that in the differential equations. It may be worth noting that the Bélanger formula cannot be derived from the non-conservative equations [11], hence the non-conservative equations are not suitable for flows including a hydraulic jump.

2.3. Solution method

A uniform staggered grid (Figure 2) is used, and the convection terms can be treated in a wide range of ways, such as LUDS and QUICK schemes. Here, the widely used power law is applied [22]. Equations (2) and (3) can be discretised by means of the finite volume approach as [17]:

$$a_P u_P = a_E u_E + a_W u_W + a_S u_S + a_N u_N + a_0, \tag{13}$$

$$b_P v_P = b_E v_E + b_W v_W + b_S v_S + b_N v_N + b_0, \tag{14}$$

where, referring to Figure 2,

$$a_E = \frac{(hv_t)_e \Delta y}{\Delta x} \max\left\{0, \left(1 - \frac{0.1|u_e|\Delta x}{v_{te}}\right)^5\right\} + \max\{0, -(hu)_e \Delta y\}, \tag{15}$$

$$a_W = \frac{(hv_t)_w \Delta y}{\Delta x} \max\left\{0, \left(1 - \frac{0.1|u_w|\Delta x}{v_{tw}}\right)^5\right\} + \max\{0, (hu)_w \Delta y\}, \tag{16}$$

$$a_N = \frac{(hv_t)_n \Delta x}{\Delta y} \max\left\{0, \left(1 - \frac{0.1|v_n|\Delta y}{v_{tn}}\right)^5\right\} + \max\{0, -(hv)_n \Delta x\}, \tag{17}$$

$$a_S = \frac{(hv_t)_s \Delta x}{\Delta y} \max\left\{0, \left(1 - \frac{0.1|v_s|\Delta y}{v_{ts}}\right)^5\right\} + \max\{0, (hv)_s \Delta x\}, \tag{18}$$

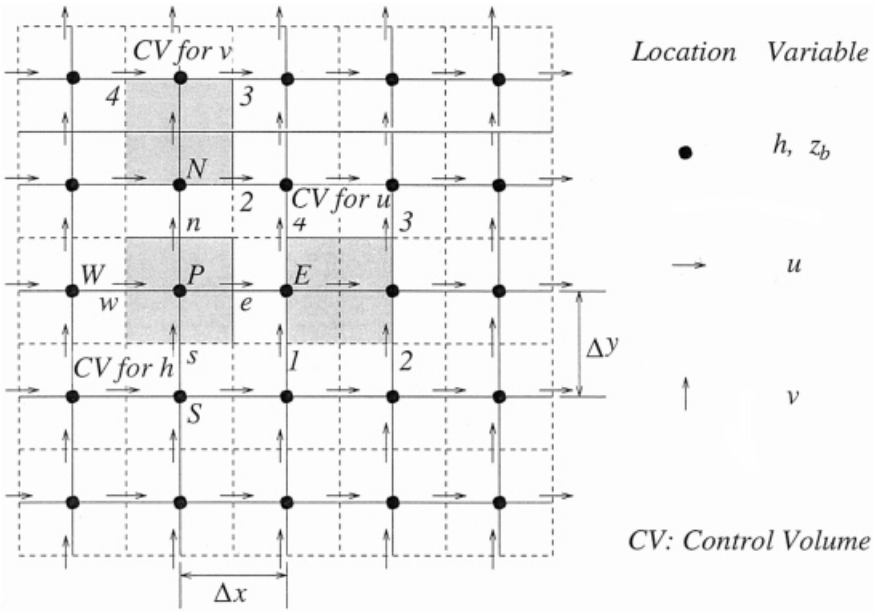

Figure 2. Grid layout and control volumes.

$$a_0 = -\frac{g}{2}\Delta y(h_e^2 - h_w^2) - g\frac{h_e + h_w}{2}\Delta y(z_e - z_w), \tag{19}$$

$$a_{\mathrm{P}} = a_{\mathrm{E}} + a_{\mathrm{W}} + a_{\mathrm{N}} + a_{\mathrm{S}} + C_{\mathrm{b}}\Delta x\Delta y\sqrt{u_{\mathrm{P}}^2 + \bar{v}_{\mathrm{P}}^2}, \tag{20}$$

$$\bar{v}_{\mathrm{P}} = \frac{v_1 + v_2 + v_3 + v_4}{4}, \tag{21}$$

$$b_{\mathrm{E}} = \frac{(hv_{\mathrm{t}})_e\Delta y}{\Delta x}\max\left\{0, \left(1 - \frac{0.1|u_e|\Delta x}{v_{\mathrm{t}e}}\right)^5\right\} + \max\{0, -(hu)_e\Delta y\}, \tag{22}$$

$$b_{\mathrm{W}} = \frac{(hv_{\mathrm{t}})_w\Delta y}{\Delta x}\max\left\{0, \left(1 - \frac{0.1|u_w|\Delta x}{v_{\mathrm{t}w}}\right)^5\right\} + \max\{0, (hu)_w\Delta y\}, \tag{23}$$

$$b_{\mathrm{N}} = \frac{(hv_{\mathrm{t}})_n\Delta x}{\Delta y}\max\left\{0, \left(1 - \frac{0.1|v_n|\Delta y}{v_{\mathrm{t}n}}\right)^5\right\} + \max\{0, -(hv)_n\Delta x\}, \tag{24}$$

$$b_{\mathrm{S}} = \frac{(hv_{\mathrm{t}})_s\Delta x}{\Delta y}\max\left\{0, \left(1 - \frac{0.1|u_s|\Delta y}{v_{\mathrm{t}s}}\right)^5\right\} + \max\{0, (hv)_s\Delta x\}, \tag{25}$$

$$b_0 = -\frac{g}{2}\Delta x(h_n^2 - h_s^2) - g\frac{h_n + h_s}{2}\Delta x(z_n - z_s), \tag{26}$$

$$b_{\mathrm{P}} = b_{\mathrm{E}} + b_{\mathrm{W}} + b_{\mathrm{N}} + b_{\mathrm{S}} + C_{\mathrm{b}}\Delta x\Delta y\sqrt{\bar{u}_{\mathrm{P}}^2 + v_{\mathrm{P}}^2}, \tag{27}$$

$$\bar{u}_{\mathrm{P}} = \frac{u_1 + u_2 + u_3 + u_4}{4}. \tag{28}$$

The depth–velocity coupling is achieved by the SIMPLE-like scheme proposed by Zhou [17]. Based on the continuity equation (1), the depth correction, h' can be obtained by solving

$$c_{\mathrm{P}}h'_{\mathrm{P}} = c_{\mathrm{E}}h'_{\mathrm{P}} + c_{\mathrm{W}}h'_{\mathrm{P}} + c_{\mathrm{N}}h'_{\mathrm{P}} + c_{\mathrm{S}}h'_{\mathrm{P}} + c_0, \tag{29}$$

where

$$c_E = (h_P^* + h_E^*)\Delta y d_{eh}, \qquad c_W = (h_P^* + h_W^*)\Delta y d_{wh}, \tag{30}$$

$$c_N = (h_P^* + h_N^*)\Delta x d_{nh}, \qquad c_S = (h_P^* + h_S^*)\Delta x d_{sh}, \tag{31}$$

$$c_P = c_E + c_W + c_N + c_S, \tag{32}$$

$$c_0 = [(h_P^* + h_E^*)u_e^* - (h_P^* + h_W^*)u_w^*]\Delta y + [(h_P^* + h_N^*)v_n^* - (h_P^* + h_S^*)v_s^*]\Delta x, \tag{33}$$

in which the superscript * denotes the values of a quantity from the latest iteration.

Equations (13) and (14) are solved first to obtain the velocities for a given depth. Then the depth correction, h' is obtained by solving Equation (29). Finally, the velocities and depth are updated according to the depth correction. This computation is repeated until convergence is reached. The detailed procedure is given in [17].

2.4. Boundary conditions

The velocity field or discharge may always be specified as an inflow boundary condition, whereas the boundary condition for the depth will be defined differently according to the flow state. Generally, the depth should be set at the upstream end for supercritical flow, but at the downstream end for subcritical flow. For critical flow, the depth may be given at either the upstream or the downstream end. Since a hydraulic jump includes a transition from super- to subcritical flow, the depth should be defined at the upstream end for the supercritical flow and also at the downstream end for the subcritical flow. These are the boundary conditions for the present model to predict a hydraulic jump.

3. VERIFICATION OF THE MODEL

As indicated in Section 2.2, the model has a shock-capturing feature. Once the correct boundary conditions are set up, there will be no special considerations for the model to predict a hydraulic jump. In order to test the validity of the model, three numerical experiments are carried out: the hydraulic jump for which there are both experimental data and numerical results by 1D and 2D flow models, a flow consisting of a hydraulic jump and a hydraulic drop, and the effect of bed roughness on a hydraulic jump.

3.1. Hydraulic jump in straight channel

The dimensions of the straight rectangular channel are 14.1 m long and 0.46 m wide; the inflow Froude number is $Fr = 2.3$. The boundary conditions are: (1) the inflow velocities $u = 1.92$ m s^{-1}, and $v = 0$; the depth $h = 0.064$ m; (2) the outflow depth $h = 0.168$ m. All these values are taken from the experimental conditions [5]. The whole domain is divided as 47×5 cells with $\Delta x = 0.3$ m and $\Delta y = 0.092$ m.

Figure 3 shows the numerical results and the experimental data. Except for two points at the top of the hydraulic jump, the agreement with experimental data is satisfactory. The figure also shows the numerical results from the 1D model by Gharangik and Chaudhry [5] and the 2D model by Molls and Chaudhry [14], showing similar agreement.

The 1D model described in [5] involves the Boussinesq term as well as an artificial viscosity, which plays the role of a fitting factor. The 2D model in [14] uses the alternating direction implicit (ADI) method and the conservation properties of the original equations are not

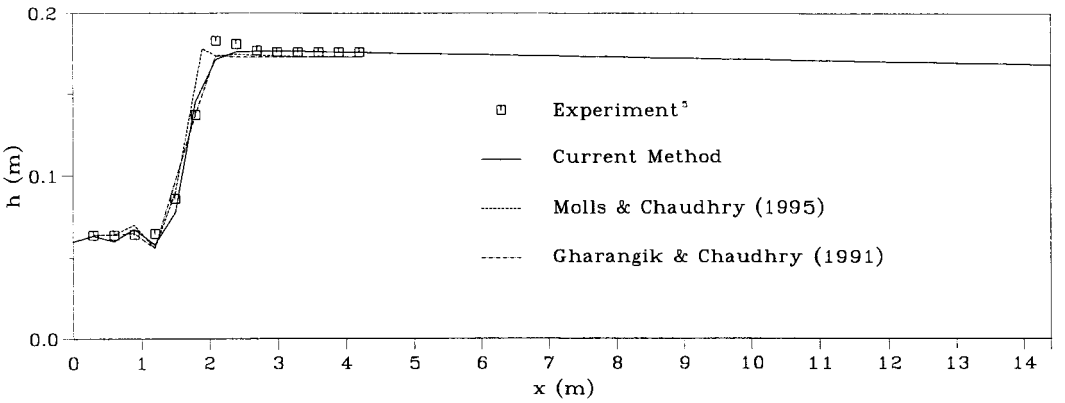

Figure 3. Comparison of numerical results and experimental data.

guaranteed. In addition, it includes an artificial viscosity and needs an outflow boundary condition for velocity as well as the depth. Thus, the present model gives good results without artificial parameters, probably because the model is based on the flow equations in strong conservation form.

3.2. Hydraulic jump and hydraulic drop

The hydraulic drop is another basic physical phenomenon in natural river or open channel flows. Unlike a hydraulic jump, in which an abrupt increase of water surface occurs, it is characterised by a substantial decrease of water depth within a short distance along the flow direction when the flow changes from the subcritical to supercritical state. According to open channel hydraulics [3], both the hydraulic jump and the hydraulic drop will occur if the inflow is in the supercritical state in a fairly long channel, with a mild bed slope, followed by a fairly long channel with a steep bed slope. Such a complex flow forms a useful test problem.

The straight rectangular channel consists of two reaches with different slopes: an upstream horizontal reach ($S = 0$), followed by a reach with a steep slope ($S = 0.03$). The first reach is 14.5 m long, and the second is 16.0 m. Both are 1.4 m wide (Figure 4).

The entrance velocities and depth are $u = 3.571\ \mathrm{m\,s^{-1}}$, $v = 0\ \mathrm{m\,s^{-1}}$ and $h = 0.06$ m, and the corresponding entrance Froude number is $Fr = 4.65$; no exit boundary condition for depth is needed because there is a critical depth in the cross-section at the change in the slope, which

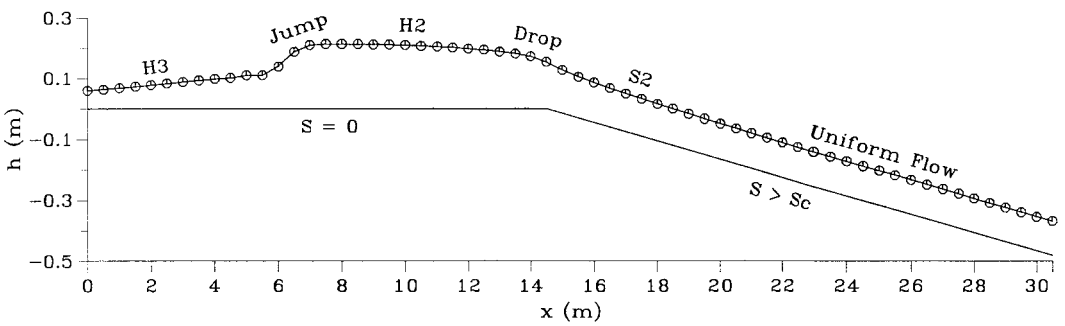

Figure 4. Profile of the central depth in hydraulic jump and drop.

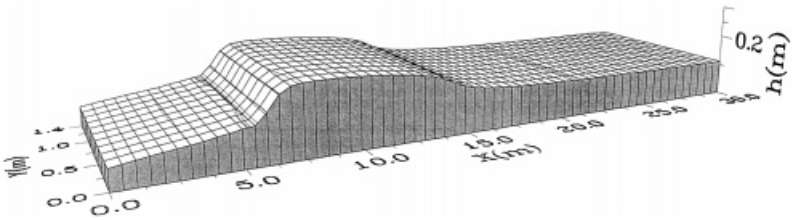

Figure 5. 3D surface of hydraulic jump and drop.

automatically plays the part of the internal boundary condition for both hydraulic jump upstream and supercritical flow downstream.

The following numerical parameters were used in the computations: $\Delta x = 0.5$ m, $\Delta y = 0.14$ m; Manning's coefficient $n = 0.019$.

Figure 4 shows the profile of the central depth in the channel. As expected, the profile consists of a H3 curve, a hydraulic jump, a H2 curve, a hydraulic drop, a S2 curve and uniform flow.

Theoretically, a hydraulic jump will occur when the upstream Froude number Fr_1, depth h_1 and downstream depth h_2 satisfy the Bélanger formula (12). This can be used to check the results by the model. From the numerical results, the upstream Froude number, depth and downstream depth of the jump are $Fr_1 = 1.7147$, $h_1 = 0.1107$ m and $h_2 = 0.2156$ m respectively. Substitution of $Fr_1 = 1.7147$ and $h_1 = 0.1107$ m into Equation (12) results in the theoretical downstream depth required for the jump as $\hat{h}_2 = 0.2187$ m. h_2 is thus very close to the theoretical downstream depth $\hat{h}_2$. The relative error is 1.4%.

In addition, the hydraulic drop occurs in the region around the change in slope and the central water depth ($h = 0.1644$ m) at the change is very close to the theoretical critical depth ($h_c = 0.1673$ m) calculated from the critical depth equation $h_c = \sqrt[3]{Q^2/gw^2}$ (where w is the width of the channel). After the hydraulic drop, the flow quickly approaches uniform flow along the second reach. The depth at the downstream end of the channel is $h = 0.1107$ m, compared with a normal depth $h_n = 0.1054$ m calculated from the Manning formula for uniform flows [3].

The 3D water surface for the hydraulic jump and drop is plotted in Figure 5. It is clearly seen from the figure that there is little transverse difference in the depth in the channel.

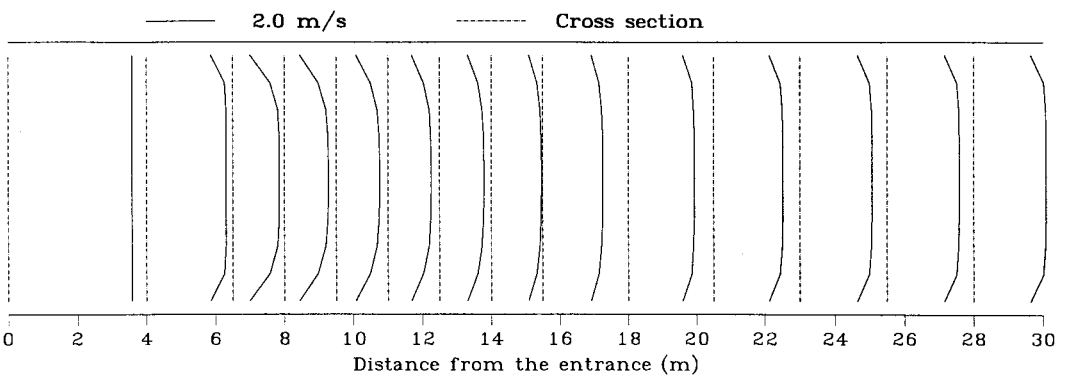

Figure 6. Distribution of velocity u. Note the velocity u at the side wall is not computed on a staggered mesh.

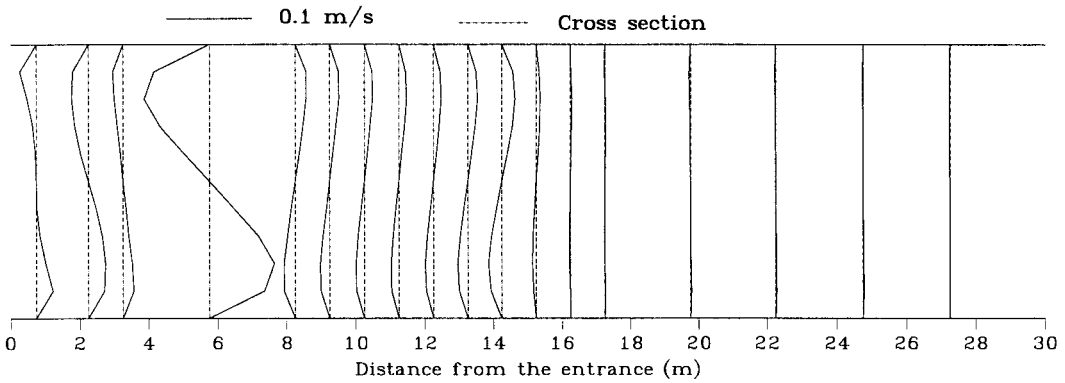

Figure 7. Distribution of velocity v.

Figures 6 and 7 show the velocity distributions. The velocity u decreases slowly before the hydraulic jump, but rapidly within the jump. After that, it increases along the flow direction, particularly fast within the hydraulic drop. The transverse velocities v have relatively large magnitudes in the regions within the hydraulic jump, as well as in the upstream reach of the hydraulic drop, such that they should not be ignored. It is clearly observed that there is a relatively strong transverse variation in the area upstream of a hydraulic jump compared with the hydraulic drop. The velocity vectors are shown in Figure 8.

3.3. Effect of bed roughness on hydraulic jump

According to open channel hydraulics, if flow rate remains unchanged, the location of a hydraulic jump will move backward (upstream against the flow direction) or forward (downstream in the flow direction) depending on increasing or decreasing of bed roughness in a channel.

The results for $n = 0.017$, 0.019 and 0.024 are plotted in Figure 9. Around the change in the slope, the flows pass through the critical depth. After the hydraulic jump, the bigger the Manning's coefficient or the rougher the bed, the greater the depth downstream of the jump.

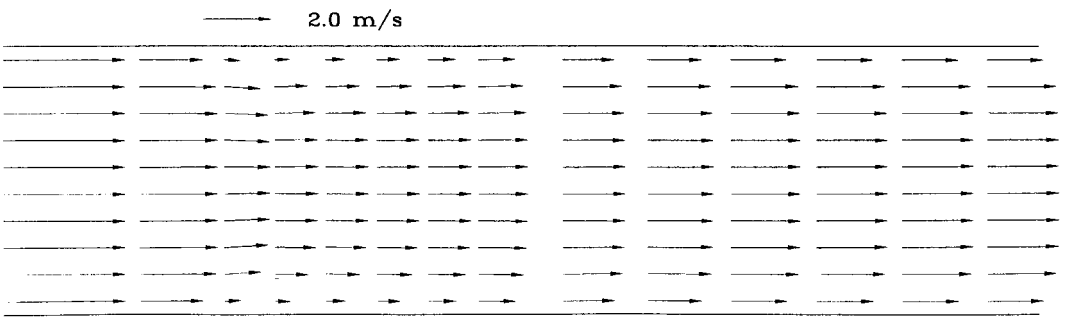

Figure 8. Velocity vectors in hydraulic jump and drop.

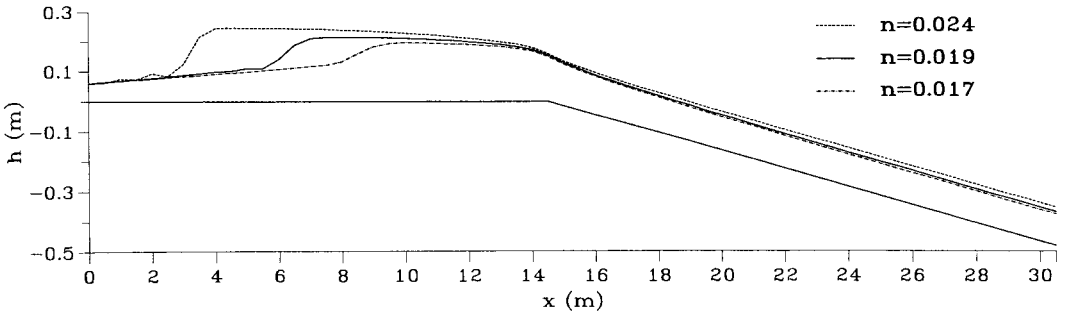

Figure 9. Effect of bed roughness on hydraulic jump and drop.

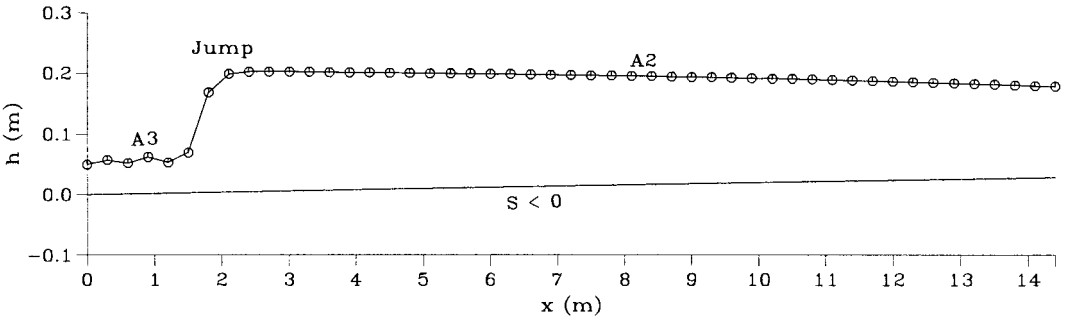

Figure 10. Hydraulic jump in channel with adverse slope.

4. FURTHER EXAMPLES

Figure 10 shows that a hydraulic jump occurs in a channel with an adverse slop ($S = -0.002$ and $n = 0.01$). The channel is 0.46 m wide and 14.1 m long. The entrance depth and Froude number are $h = 0.05$ m and $Fr = 3.3651$ respectively; the discharge $Q = 0.053$ m^3 s^{-1} and the downstream depth is $h = 0.15$ m. As shown in the figure, the flow profile consists of an A3 curve upstream, a jump and an A2 curve downstream.

In Figure 11, a hydraulic jump is simulated in a channel with a mild slope ($S = 0.002$ and $n = 0.01$). The channel is the same as that in Figure 10. The entrance depth and Froude number are $h = 0.064$ m and $Fr = 2.3237$ respectively; the discharge $Q = 0.053$ m^3 s^{-1}, and the downstream depth is $h = 0.15$ m. The figure shows the flow profile: a M3 curve upstream, a jump and a M1 curve, which agrees with that of a flow over a mild bed slope.

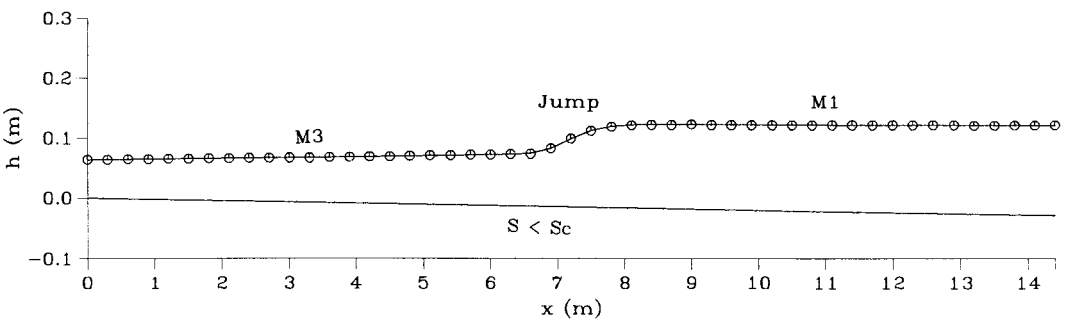

Figure 11. Hydraulic jump in channel with mild slope.

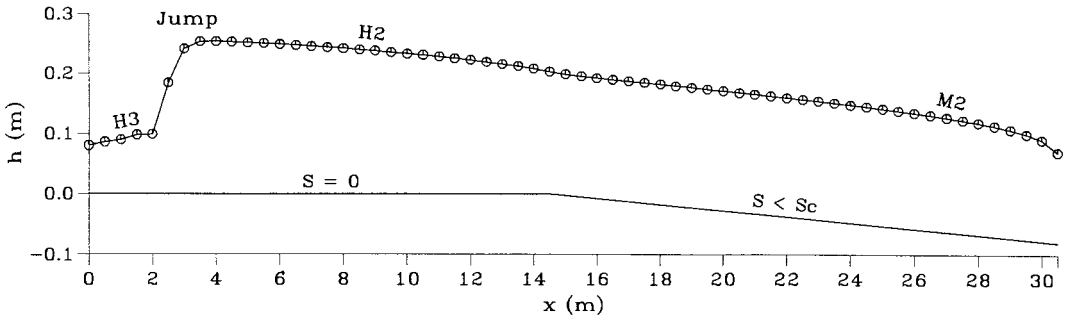

Figure 12. Hydraulic jump in channel with slope change from horizontal to mild.

Figure 12 shows a hydraulic jump in a channel with two different slopes: the upstream slope is horizontal ($S = 0.0$), with a length of 14.5 m and the downstream slope is mild ($S = 0.005$), with a length of 16.0 m. The Manning's coefficient is $n = 0.02$, and both sections are 1.4 m wide. The entrance depth and Froude number are $h = 0.08$ m and $Fr = 3.0251$ respectively; the discharge $Q = 0.3$ m^3 s^{-1} and the downstream depth is $h = 0.15$ m.

Figure 13 shows a hydraulic jump in a channel with two different slopes: the upstream slope is steep ($S = 0.04$), with a length of 28.0 m and the downstream slope is mild ($S = 0.002$), with length of 28.56 m. The Manning's coefficient is $n = 0.02$, and both are 1.4 m wide. The entrance depth and Froude number are $h = 0.48$ m and $Fr = 1.0292$ respectively; the discharge $Q = 1.5$ m^3 s^{-1} and the downstream depth is $h = 0.5$ m. The hydraulic jump occurs in the second reach of the channel with the mild slope.

In the final application, a hydraulic jump is predicted in a channel with two different slopes: the upstream slope is steep ($S = 0.02$) and the downstream slope is adverse ($S = -0.005$). The other conditions are the same as that in Figure 13. The entrance Froude number and depth are $Fr = 1.0669$ and $h = 0.21$ m respectively; the discharge is $Q = 0.45$ m^3 s^{-1} and the downstream depth is $h = 0.21$ m. The profile is plotted in Figure 14. This hydraulic jump occurs in the upstream reach of the channel with the steep slope.

5. CONCLUSIONS

A shallow water flow model that allows for hydraulic jumps is described. There is no artificial viscosity or Boussinesq term in the model. This generalises the application of the model to

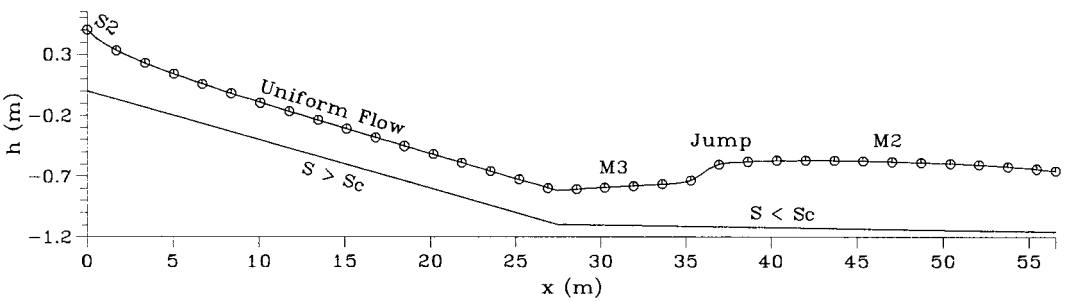

Figure 13. Hydraulic jump in channel with slope change from steep to mild.

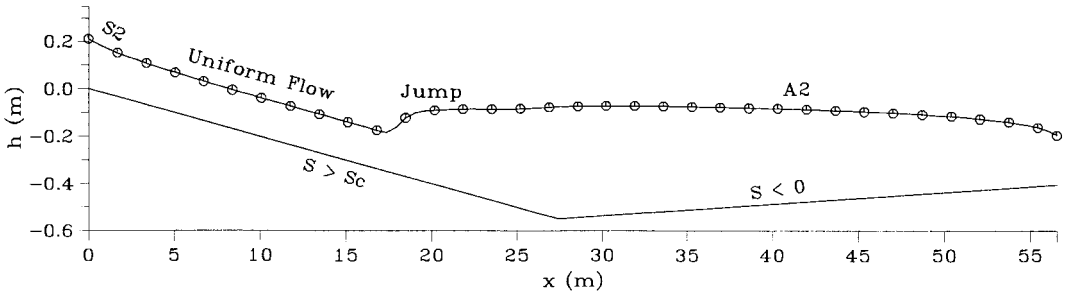

Figure 14. Hydraulic jump in channel with slope change from steep to adverse

different hydraulic situations. The study has indicated that the predictions by the present model are in good agreement with experimental data and theoretical results. The model retains the same global conservation properties as the original differential equations. It has been shown how the model may be applied to various situations. The method may be extended to simulate a hydraulic jump occurring in a channel with an arbitrary boundary shape with body-fitted co-ordinates in the future.

APPENDIX A. NOMENCLATURE

C_b	bed friction coefficient
C_z	Chezy coefficient
Fr	Froude number $Fr = u/\sqrt{gh}$
g	gravitational acceleration ($= 9.8$ m^2 s^{-1})
h	water depth
h_c	critical depth
k	von Kármán constant ($= 0.4$)
n	Manning's coefficient
Q	discharge
q	discharge per unit width
S	bottom slope in prismatic channel
S_c	critical bottom slope in prismatic channel
u_*	shear velocity
u, v	depth-averaged components of velocity in x- and y-directions respectively
x, y	Cartesian co-ordinates
z_b	elevation of channel bed
ν_t	depth-averaged turbulent viscosity
ρ	fluid density
τ_w	shear stress at the wall
τ_{bx}, τ_{by}	bed shear stresses in x- and y-directions
Δ	difference quantity

REFERENCES

1. W.H. Hager, *Energy Dissipators and Hydraulic Jump*, Kluwer, Dordrecht, 1992.
2. J.M. Bélanger, *Essai sur la Solution Numerique de Quelques Problemes, Relatives au Mouvement Permanent des Eaux Courantes*, Paris, 1828.
3. V.T. Chow, *Open Channel Hydraulics*, McGraw-Hill, New York, 1959.
4. N. Rajaratnam, 'Hydraulic jumps', *Adv. Hydrosci.*, **4**, 197–280 (1967).
5. A.M. Gharangik and M.H. Chaudhry, 'Numerical simulation of hydraulic jump', *J. Hydr. Eng. Div. ASCE*, **117**, 1195–1211 (1991).
6. F.E. Hicks and P.M. Steffler, 'Characteristic dissipative Galerkin scheme for open channel flow', *J. Hydr. Eng. Div. ASCE*, **118**, 337–352 (1992).
7. P. Garcia-Navarro, P. Priestley and F. Alcrudo, 'An implicit method for water flow modeling in channels and pipes', *J. Hydr. Res.*, **5**, 721–742 (1994).
8. M. Rahman and M.H. Chaudhry, 'Simulation of hydraulic jump with grid adaptaion', *J. Hydr. Res.*, **33**, 555–569 (1995).
9. D. Long, P.M. Steffler and N Rajaratnam, 'A numerical study of submerged hydraulic jumps', *J. Hydr. Res.*, **29**, 293–308 (1991).
10. S. Chippada, B. Ramaswamy and M.F. Wheeler, 'Numerical simulation of hydraulic jump', *Int. J. Numer. Methods Eng.*, **37**, 1381–1397 (1994).
11. J.G. Zhou, A mathematical model for shallow water flows with sediment transport, *Ph.D. Thesis*, Leeds University, UK, 1997.
12. Q. Liu and U. Drewes, 'Turbulence characteristics in free and forced hydraulic jumps', *J. Hydr. Res.*, **32**, 877–898 (1994).
13. M. Younus and M. Chaudhry, 'A depth averaged k–ϵ model for the computation of free surface flow', *J. Hydr. Res.*, **32**, 415–444 (1994).
14. T. Molls and M.H. Chaudhry, 'Depth-averaged open channel flow model', *J. Hydr. Eng. Div. ASCE*, **121**, 453–465 (1995).
15. A.A. Khan and P.M. Steffler, 'Physically based hydraulic jump model for depth-averaged computations', *J. Hydr. Eng. Div. ASCE*, **122**, 540–548 (1996).
16. T.T. Siao, H. Rouse and S. Nagaratnam, 'Turbulence characteristics of the hydraulic jump', *J. Hydr. Eng. Div. ASCE*, **84**, 1528–1530 (1958).
17. J.G. Zhou, 'Velocity-depth coupling in shallow water flows', *J. Hydr. Eng. Div. ASCE*, **121**, 717–724 (1995).
18. J.G. Zhou, 'Numerical simulation of flows in open channels', In C. Taylor and P. Durbetaki (eds.), *Numerical Methods in Laminar and Turbulent Flow*, vol. 9, part 2, Pineridge Press, UK, 1995, pp. 917–928.
19. J.G. Zhou and I.M. Goodwill, 'A finite volume method for steady state 2D shallow water flows', *Int. J. Numer. Methods Heat Fluid Flow*, **7**, 4–23 (1997).
20. R.E. Featherstone and C. Nalluri, *Civil Engineering Hydraulics*, 3rd edn., Hartnolls, Bodmin, Cornwall, UK, 1995.
21. J.W. Elder, 'The dispersion of marked fluid in turbulent shear flow', *J. Fluid Mech.*, **5**, 544–560 (1959).
22. S.V. Patankar, *Numerical Heat Transfer and Fluid Flow*, Hemisphere, New York, NY, 1980.

